

Topological frequency shift of quantum oscillation in CaFeAsF

Taichi Terashima,^{1,*} Shinya Uji,¹ Teng Wang,^{2,3} and Gang Mu^{2,3,†}

¹*International Center for Materials Nanoarchitectonics,
National Institute for Materials Science, Tsukuba 305-0003, Japan*

²*State Key Laboratory of Functional Materials for Informatics,
Shanghai Institute of Microsystem and Information Technology,
Chinese Academy of Sciences, Shanghai 200050, China*

³*CAS Center for Excellence in Superconducting
Electronics (CENSE), Shanghai 200050, China*

(Dated: May 16, 2022)

Abstract

Shubnikov-de Haas oscillation measurements were performed on CaFeAsF up to a high temperature of $T = 9$ K. The oscillation frequency of the α Dirac electron cylinder exhibits a negative shift as the temperature is raised, while that of the β Schrödinger hole cylinder shows a positive shift. At high temperatures ($T \geq 5$ K) where the β oscillation is negligible, the shift of the α frequency is proportional to T^2 and its magnitude agrees within experimental accuracy with the topological frequency shift proposed by Guo, Alexandradinata, *et al.* (arXiv:1910.07608), who argues that the energy dependence of the effective mass peculiar to a linear band dispersion of Dirac/Weyl fermions gives rise to a frequency shift proportional to T^2 . At low temperatures where the β oscillation is not negligible, the two frequencies (α and β) could not be determined so accurately as to allow quantitative comparison to the theory.

Keywords: quantum oscillation, Dirac fermions, Weyl fermions, iron-based superconductor, topological material, Shubnikov-de Haas effect, CaFeAsF, de Haas-van Alphen effect

Classifications: 106 Metallic materials - 40 Optical, magnetic and electronic device materials

* TERASHIMA.Taichi@nims.go.jp

† mugang@mail.sim.ac.cn

Quantum oscillation arising from Landau quantization of electron motion in magnetic fields is a powerful tool to investigate electronic structures of metals. It dates back to 1930 when quantum oscillation in the electrical resistance and magnetization in Bi was observed [1, 2]. Since the Onsager relation [3] and Lifshitz-Kosevich formula [4] to interpret the quantum oscillation were established in 1950s, it has been used to determine the Fermi surface of not only elemental metals [5] but also heavy fermions [6, 7], high-Tc cuprates [8], and so on. The latest field of its application is topological materials. Topological surface states of topological insulators were successfully observed in quantum-oscillation measurements [9, 10]. Further, Dirac or Weyl fermions in topological semimetals can in principle be identified by detecting the Berry phase in quantum-oscillation measurements [11, 12]. However, the necessary procedure is involved even if it is not impossible to perform.

To be specific, we focus on Shubunikov-de Haas (SdH) oscillation, which is described as follows [5, 13]:

$$\frac{\Delta\rho}{\rho_0} = -C\sqrt{B}R_T R_D R_s \cos\left[2\pi\left(\frac{F}{B} - \frac{1}{2}\right) + \phi_D + \phi_B\right], \quad (1)$$

where $\Delta\rho$ is the oscillatory part of resistivity, while ρ_0 is the background resistivity. We have neglected harmonics. C is a positive coefficient. The frequency F is related to a Fermi-surface cross sectional area A as $F = (\hbar/2\pi e)A$. The temperature and Dingle reduction factors are given by $R_T = X/\sinh X$ and $R_D = \exp(-X_D)$, where $X_{(D)} = K\mu^*T_{(D)}/B$, $\mu^* = m^*/m_e$, and the coefficient K is 14.69 T/K. The spin reduction factor R_s describes the interference of oscillations from up- and down-spin electrons and is given by $R_s = \cos(\pi g\mu^*/2)$, where g is the conduction-electron g factor averaged over the cyclotron orbit under consideration. ϕ_D is 0 for a two-dimensional (2D) Fermi-surface (FS) cylinder while it is $+$ or $-\pi/4$ when the oscillation is from a minimum or maximum cross section of a three-dimensional (3D) FS pocket. ϕ_B is the Berry phase, which is 0 for normal (i.e., Schrödinger) fermions but π for Dirac fermions [11, 12].

We note that the phase of quantum oscillation is the same between normal fermions with a negative R_s and Dirac fermions with a positive R_s . Therefore, if we like to determine the Berry phase from experimental data by making a Landau-index plot or fitting Eq. 1 to the data, we first have to determine the sign of R_s . R_s depends on g and m^* . g may substantially deviate from the free-electron value $g = 2$, especially for small orbits: e.g. for the Zn needle, $g > 100$ is generally accepted [5]. g could be determined by e.g. the spin-zero

method in some special cases [14], but it is impossible in many cases. Note that even in noncentrosymmetric crystals, in which double degeneracy of electronic bands is lifted, R_s (or its equivalent) has to be considered as long as time-reversal symmetry is preserved because oscillations from a time-reversal pair of orbits interfere [15].

Recently, Guo, Alexandradinata, *et al.* (hereafter GAM *et al.* after the three corresponding authors) proposed a new approach [16]. They pointed out that quantum-oscillation frequency from Dirac/Weyl pockets should exhibit a characteristic temperature dependence. The cyclotron effective mass m^* is defined as $m^* = (\hbar^2/(2\pi))|\partial A/\partial E|$. Accordingly, $\partial m^*/\partial E$ is zero for a quadratic band dispersion but finite for a linear dispersion: assuming $E = \hbar vk$, where v is the Fermi velocity, $m^* = |E|/v^2$ and $|\partial m^*/\partial E| = 1/v^2$, that is, as $|E|$ decreases both A and m^* decrease. At a finite temperature T , the Fermi edge broadens, and hence the system might be viewed as a sum of hypothetical systems with the Fermi energy distributed over a range of $\sim k_B T$ around E_F . Since oscillation from smaller orbits with smaller m^* survives to higher temperatures, the effective frequency might decrease. They extended the Lifshitz-Kosevich formula to the next order in $k_B T/E_F$ and showed that the above expectation is indeed the case (see also [17]):

$$F(T) = F_0 - \frac{(\pi k_B T)^2}{4\beta} \frac{1}{m^*} \left| \frac{\partial m^*}{\partial E} \right|, \quad (2)$$

where F_0 is the frequency at $T = 0$ and $\beta = e\hbar/(2m^*)$. They analyzed quantum oscillation from Dirac pockets in Cd_3As_2 and LaRhIn_5 and demonstrated that Eq. 2 combined with another small correction to $F(T)$, which will be described later, could explain the experimentally observed temperature dependence of the frequencies.

In this article, we apply the GAM method to SdH oscillation in CaFeAsF , an iron-base superconductor parent compound. The Fermi surface in CaFeAsF is composed of a pair of α Dirac electron cylinders and a β Schrödinger hole cylinder [14]. By virtue of the quasi-two-dimensional electronic structure, the sign of R_s was unambiguously determined for both α and β orbits in our previous SdH study and the Berry phase π (0) was confirmed for α (β) orbits. In the present study, we perform new SdH measurements up to higher temperatures, aiming to extract the temperature dependence of the α and β frequencies and to compare them to the GAM model.

CaFeAsF single crystals #0618, #0811, and #1012 were prepared in Shanghai by a CaAs self-flux method [18]. The resistivity was measured along the c axis, and the magnetic field

up to 17.5 T was applied along the c axis. A dilution refrigerator with a base temperature of 0.03 K was used, and the maximum measurement temperature was 1.8 , 9, and 7 K for sample #0618, #0811, and #1012, respectively (sample #0618 was measured first, and we did not notice that higher temperatures were necessary). At each set temperature, the magnetic field was ramped up to 17.5 T and then down to zero, and thus two magnetoresistivity curves (B -up and B -down) were obtained. No hysteresis was observed and B -up and B -down curves agreed well at all temperatures.

Figure 1 shows the (B -up) magnetoresistivity, second field derivative, and Fourier transform of $d^2\rho/dB^2$ vs $1/B$ for the three samples. SdH oscillations are visible in all the samples. The Fourier transform of the second derivative in $1/B$ shows the two peaks corresponding to the α and β frequencies. The insets show the temperature dependences of the oscillation amplitudes. The amplitude error bars are based on the background amplitude observed in the spectra at higher frequencies than α and β , while the temperature error is assumed to be 5%. By orthogonal distance regression fitting to the temperature reduction factor R_T (solid lines), we estimate effective masses and associated errors as shown in Table I. The obtained values are mutually consistent and also consistent with our previous result [14].

In order to precisely determine the frequencies at each temperature, we fit experimental data ρ_{exp} assuming that each oscillatory component follows Eq. 1. We explain our fitting procedure with Fig. 2, which shows fitting results at selected temperatures for sample #0811. The fit function is $\rho_{\text{fit}} = \rho_0(1 + \Delta\rho_\alpha/\rho_0 + \Delta\rho_\beta/\rho_0)$, where ρ_0 is given by a second-order polynomial. As determined in our previous study [14], R_s is positive and $\phi_D = 0$ for both frequencies, while $\phi_B = \pi$ and 0 for α and β , respectively. We fix the effective masses as estimated above: $m_\alpha^*/m_e = 0.43$, and $m_\beta^*/m_e = 0.89$ for sample #0811. The remaining parameters are F , T_D , and a proportionality factor C' ($=CR_s$) for each component. We first fit the average of the B -up and B -down data at $T = 0.03$ K above $B = 5$ T with those free fitting parameters. The obtained frequencies are assumed to be the zero-temperature frequencies F_o (Table I). We then fit B -up and B -down data, separately, at each set temperature (Fig. 2) with the values of T_D and C' fixed at those obtained at $T = 0.03$ K (Table I): accordingly there is only one fitting parameter F for each component at each temperature. The β component is largely suppressed as the temperature is raised to $T = 1.82$ K (Fig. 2). At $T = 3.0$ K and above, whether β is included or not does not affect the quality of fit and hence we omit β . We thus obtain $\Delta F_{\alpha(\beta)} = F_{\alpha(\beta)} - F_0$ at measured temperatures.

We now like to estimate the errors in the frequencies caused by the errors in the effective masses. We therefore repeat the fitting procedure but with the effective-mass values increased by the amount of the error: namely, $m_\alpha^*/m_e = 0.45$, and $m_\beta^*/m_e = 0.92$. We assume the errors in the temperature-dependent frequencies are equal to the differences between the frequencies obtained in the two fitting routines. The errors in the Dingle temperatures are also estimated by comparing results of the two routines (Table I).

Data for sample #0618 and #1012 are analyzed in the same way, and the fitting results at the base temperature are shown in Fig. 3. Figure 4 shows the obtained temperature shifts of the frequencies for the three samples. Note that there are two data points at each set temperature corresponding to B -up and B -down sweeps.

Before discussing Fig. 4, we review theoretical frequency shifts expected from the GAM model [16]. Following GAM *et al.*, we introduce a parameter Θ and rewrite Eq. 2 as follows:

$$F(T) = F_0 - \Theta \left(\frac{\pi k_B}{\mu_B} \right)^2 \frac{T^2 (\mu^*)^2}{F_0}, \quad (3)$$

where μ_B is the Bohr magneton. GAM *et al.* noted that Θ is the sum of the topological part $\Theta^T = 1/16$ and a Sommerfeld part Θ^S due to the temperature dependence of the chemical potential (Sommerfeld correction). The chemical potential shift is described by

$$\zeta(T) = E_F - \frac{1}{6} (\pi k_B T)^2 \frac{D'}{D}, \quad (4)$$

where D and D' are the zero-field density of states and its energy derivative, respectively. The corresponding frequency shift can be calculated by $\Delta F = (+/-)(m^*/(e\hbar))\Delta\zeta$ (electron/hole). When evaluating Eq. 4, all existing Fermi pockets have to be included. GAM *et al.* considered two extreme cases [16]: One is Cd_3As_2 , which has only small Dirac pockets. D is solely determined by those pockets, which gives $\Theta^S = 1/24$. The other is a tiny Dirac pocket in LaRhIn_5 , which coexists with much larger Schrödinger ones. In this case, D'/D is dominated by the latter pockets with an effective Fermi energy much larger than measurement temperatures, and hence $\Delta\zeta$ is negligibly small, i.e., $\Theta^S = 0$. The experimental frequency shifts in the two compounds were excellent agreement with those expected from the sum of Θ^T and Θ^S .

The present case is more general. We have to consider the α Dirac and β Schrödinger cylinders at the same time: $D = 2D_\alpha + D_\beta$ since there are two α cylinders in the Brillouin zone. We make a two-dimensional approximation. Then, the density of states is proportional

to the effective mass. Further, $D'_\alpha/D_\alpha = 1/E_\alpha$, and $D'_\beta = 0$. Accordingly, $D'/D = (2/(2 + (m_\beta^*/m_\alpha^*))(1/E_\alpha))$, which leads to $\Theta_\alpha^S = (1/(2+r))(1/24)$ and $\Theta_\beta^S = -(R/(2+r))(1/12)$ with $r = m_\beta^*/m_\alpha^*$ and $R = E_\beta/E_\alpha$. Using experimental values in Table I, we obtain $\Theta_\alpha = \Theta_\alpha^S + \Theta_\alpha^T = 0.0719(5)$, $0.0727(4)$, and $0.073(1)$, and $\Theta_\beta = \Theta_\beta^S = -0.011(2)$, $-0.012(2)$, and $-0.012(4)$ for sample #0618, #0811, and #1012, respectively. We show in Fig. 4 the theoretical frequency shifts calculated for sample #0811 (the shifts calculated for the other samples are almost indistinguishable from the plotted ones).

Our main results shown in Fig. 4 are qualitatively consistent with the GAM model in that, while the trivial β frequency shows a positive shift, the α frequency arising from the Dirac pockets shows a negative shift. Further, at high temperatures where the amplitude of the β oscillation is negligibly small, the experimental α frequency shifts show linear dependence on $T^2(\mu^*)^2/F_0$. Linear fits to #0811 and #1012 data points for $T \geq 5$ K (broken lines) give $\Theta = 0.081 \pm 0.015$ and 0.082 ± 0.024 , respectively, where the errors are estimated from the fitting error and the systematic error due to the error in the effective mass. The obtained values agree with the theoretical values estimated above within experimental accuracy. This observation supports the quantitative accuracy of the GAM model.

On the other hand, at low temperatures where the β oscillation is not negligible, the experimental frequency shifts largely deviate from the theoretical lines and exhibit appreciable sample dependence. We notice clear correlation between the α and β shifts for each sample: both of the α and β shifts are the largest for sample #0618 and the smallest for sample #1012. This suggests a problem in the fitting procedure of $\rho(B)$: it seems that the two frequencies interfere with each other in the fitting procedure. In the present measurements, the observed oscillation periods are a few or less, it is very likely that more oscillation periods are necessary to accurately determine the two frequencies at the same time.

To conclude, we performed SdH measurements on CaFeAsF from $T = 0.03$ K to a high temperature ($T = 9$ K for sample #0811 and 7 K for sample #1012). The SdH frequency of the α Dirac cylinder showed a T^2 shift at sufficiently high temperatures where the β oscillation is negligible, and the magnitude of the frequency shift is consistent with the topological frequency shift predicted by GAM *et al.* [16]. At low temperatures where the β oscillation is not negligible, we were unable to accurately determine the two frequencies: further measurements to observe more oscillation periods are necessary to determine the shifts of the two frequencies at low temperatures and to compare them with the GAM

model.

ACKNOWLEDGMENTS

This work was supported in Japan by JSPS KAKENHI Grant Number 17K05556. This work was supported in China by the Youth Innovation Promotion Association of the Chinese Academy of Sciences (No. 2015187).

-
- [1] Schubnikow, V. L. & de Haas, W. J. Magnetische widerstandsvergrößerung in einkristallen von wismut bei tiefen temperaturen. *Proc. Netherlands Roy. Acad. Sci.* **33**, 130 (1930).
- [2] de Haas, W. J. & van Alphen, P. M. The dependenee of the susceptibility of diamagnetic metals upon the field. *Proc. Netherlands Roy. Acad. Sci.* **33**, 1106 (1930).
- [3] Onsager, L. Interpretation of the de haas-van alphen effect. *Phil. Mag.* **43**, 1006 (1952).
- [4] Lifshitz, I. M. & Kosevich, A. Theory of magnetic susceptibility in metals at low temperatures. *Sov. Phys. JETP* **2**, 636 (1956).
- [5] Shoenberg, D. *Magnetic Oscillations in Metals* (Cambridge University Press, Cambridge, 1984).
- [6] Reinders, P. H. P., Springford, M., Coleridge, P. T., Boulet, R. & Ravot, D. de haas-van alphen effect in the heavy-electron compound CeCu_6 . *Phys. Rev. Lett.* **57**, 1631–1634 (1986).
- [7] Taillefer, L. & Lonzarich, G. G. Heavy-fermion quasiparticles in UPt_3 . *Phys. Rev. Lett.* **60**, 1570–1573 (1988).
- [8] Doiron-Leyraud, N. *et al.* Quantum oscillations and the fermi surface in an underdoped high- T_c superconductor. *Nature* **447**, 565–568 (2007).
- [9] Qu, D.-X., Hor, Y. S., Xiong, J., Cava, R. J. & Ong, N. P. Quantum oscillations and hall anomaly of surface states in the topological insulator Bi_2Te_3 . *Science* **329**, 821–824 (2010).
- [10] Analytis, J. G. *et al.* Two-dimensional surface state in the quantum limit of a topological insulator. *Nature Physics* **6**, 960–964 (2010).
- [11] Mikitik, G. P. & Sharlai, Y. V. Manifestation of Berry’s Phase in Metal Physics. *Phys. Rev. Lett.* **82**, 2147–2150 (1999).
- [12] Mikitik, G. P. & Sharlai, Y. V. Semiclassical Energy Levels of Electrons in Metals with Band Degeneracy Lines. *Soviet Physics–JETP* **87**, 747–755 (1998).
- [13] Richards, F. E. Investigation of the Magnetoresistance Quantum Oscillations in Magnesium. *Phys. Rev. B* **8**, 2552–2571 (1973).
- [14] Terashima, T. *et al.* Fermi Surface with Dirac Fermions in CaFeAsF Determined via Quantum Oscillation Measurements. *Phys. Rev. X* **8**, 011014 (2018).
- [15] Hirose, H. T. *et al.* Real spin and pseudospin topologies in the noncentrosymmetric topological nodal-line semimetal CaAgAs . *Phys. Rev. B* **101**, 245104 (2020).

- [16] Guo, C. *et al.* Fingerprint of topology in quantum oscillations at elevated temperatures. *arXiv:1910.07608* (2019).
- [17] Fortin, J.-Y. & Audouard, A. Effect of electronic band dispersion curvature on de haas-van alphen oscillations. *The European Physical Journal B* **88**, 225 (2015).
- [18] Ma, Y. *et al.* Growth and Characterization of Millimeter-Sized Single Crystals of CaFeAsF. *Supercond. Sci. Technol.* **28**, 085008 (2015).

TABLE I. Fermi-surface parameters. The zero-temperature frequencies (F_0) are estimated from Lifshitz-Kosevich fits to base-temperature data, and the associated errors are numerical fitting errors. The effective masses (m^*) are estimated from the temperature dependence of Fourier amplitudes, and the associated errors take into account the amplitude and temperature errors in experiment. The Dingle temperatures (T_D) are estimated from Lifshitz-Kosevich fits to base-temperature data, and the associated errors take into account the errors in the effective masses. See text for details of the error estimation. The Fermi energies (E_F) are derived from F_0 and m^* , using the linear dispersion relation ($E_F = \hbar v_F k_F$) for the α cylinder and a quadratic one ($E_F = \hbar^2 k_F^2 / (2m^*)$) for β .

sample	α				β			
	F_0 (T)	m^*/m_e	T_D (K)	E_F (meV)	F_0 (T)	m^*/m_e	T_D (K)	E_F (meV)
#0618	19.103(1)	0.39(3)	7.3(6)	11(1)	49.542(6)	0.94(3)	1.67(5)	6.1(2)
#0811	18.521(2)	0.43(2)	4.7(3)	10.0(5)	45.510(7)	0.89(3)	1.62(5)	5.9(2)
#1012	16.504(2)	0.40(5)	5.5(7)	10(2)	40.455(3)	0.87(8)	2.1(2)	5.4(5)

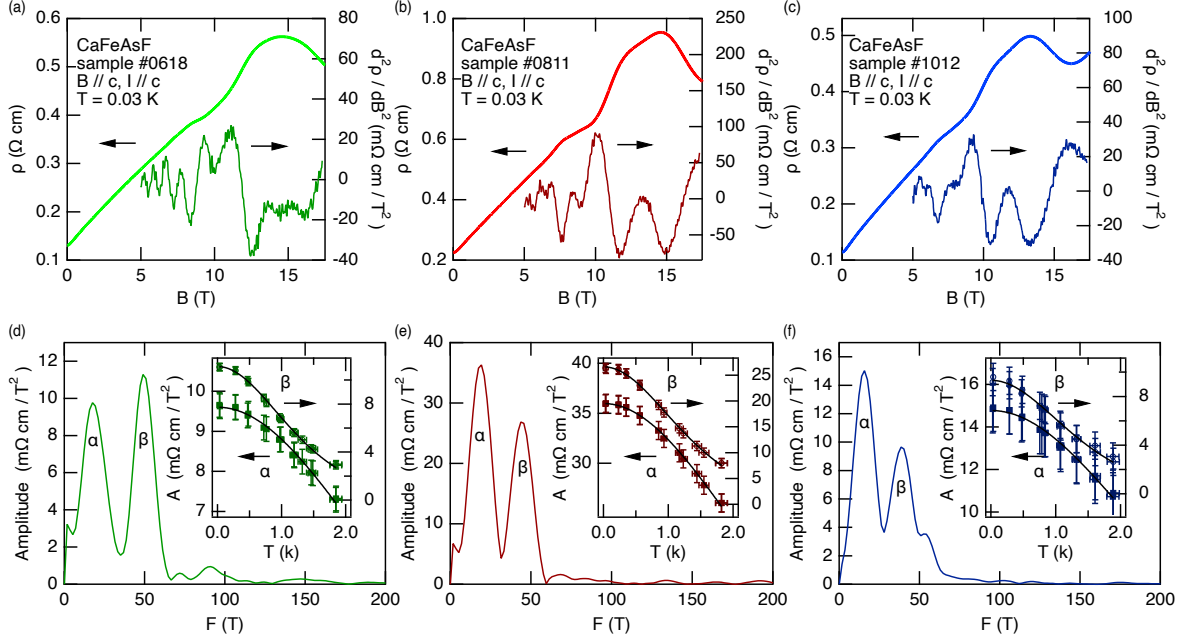


FIG. 1. (a, b, and c) Magnetoresistivity, its second field derivative, and (d, e, and f) Fourier transform of $d^2\rho/dB^2$ vs $1/B$ for samples #0618, #0811, and #1012, respectively. (insets) Temperature dependence of α and β oscillation amplitudes. The amplitude error bars are based on the noise floor of the Fourier spectra, and the temperature error bars are assumed to be 5%. The solid lines are fits to R_T .

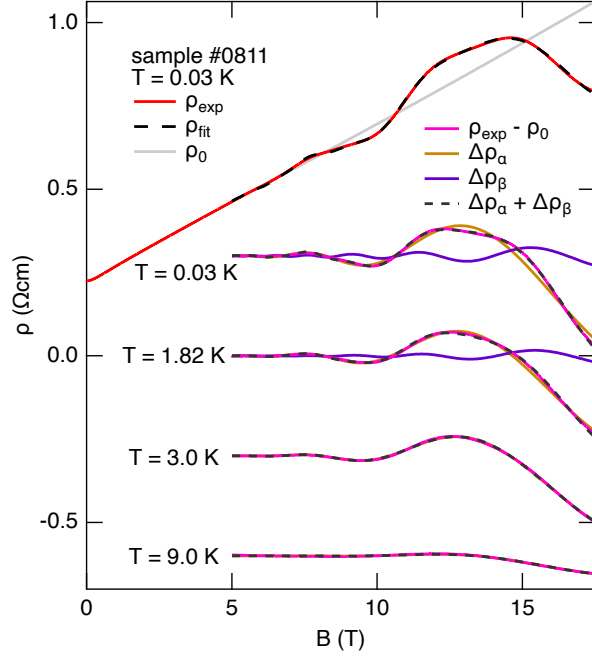


FIG. 2. Lifshitz-Kosevich fits to the magnetoresistivity in sample #0811 for selected temperatures. For $T = 0.03$ K, the total resistivity ρ_{exp} and oscillatory part $\rho_{exp} - \rho_0$, where ρ_0 is the smooth background, are shown. For the other temperatures, only the oscillatory parts are shown. The oscillatory parts are mutually shifted vertically for clarity. We omit the β component at $T = 3.0$ K and above because its inclusion does not improve the quality of fit.

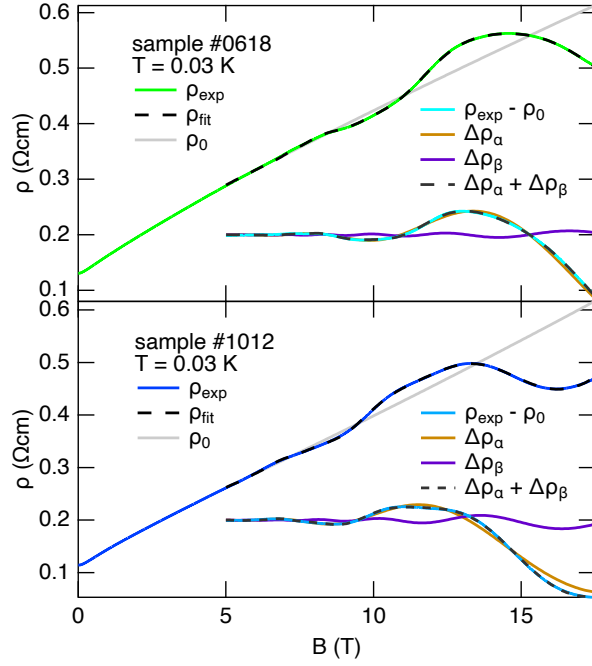


FIG. 3. Lifshitz-Kosevich fits to the magnetoresistivity in sample #0618 and #1012 at $T = 0.03$ K.

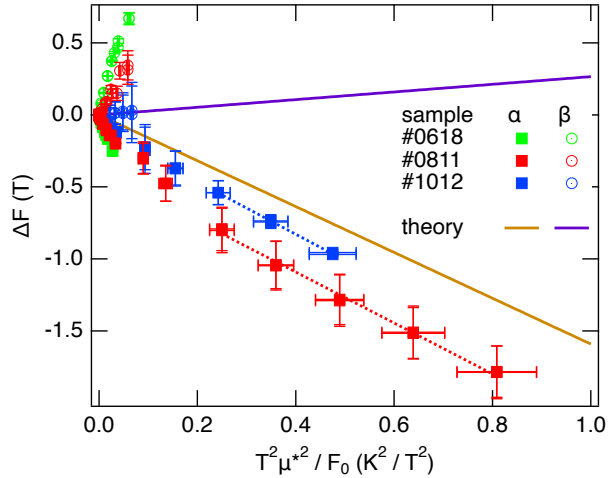


FIG. 4. Experimental (marks) and theoretical (solid lines) frequency shifts in CaFeAsF. The estimation of the vertical error bars is explained in the main text. The horizontal error bars are based on the 5% temperature error (the systematic error due to the error in μ^* is not shown). The broken lines are linear fits to data points of #0811 and #1012 for $T \geq 5$ K